EFDA–JET–CP(12)06/28

M. Lehnen, G. Arnoux, N. Hartmann, S. Brezinsek, J. Flanagan, S.N. Gerasimov,
T.C. Hender, A. Huber, S. Jachmich, U. Kruezi, G.F. Matthews, J. Morris,
V.V. Plyusnin, C. Reux, V. Riccardo, B. Sieglin, P.C. de Vries
and JET EFDA contributors

Impact and Mitigation of Disruptions with the ITER-like Wall in JET

Impact and Mitigation of Disruptions with the ITER-like Wall in JET

M. Lehnen[1], G. Arnoux[2], N. Hartmann[1], S. Brezinsek[1], J. Flanagan[2], S.N. Gerasimov[2], T.C. Hender[2], A. Huber[1], S. Jachmich[3], U. Kruezi[2], G.F. Matthews[2], J. Morris[2], V.V. Plyusnin[4], C. Reux[5], V. Riccardo[2], B. Sieglin[6], P.C. de Vries[7] and JET EFDA contributors*

JET-EFDA, Culham Science Centre, OX14 3DB, Abingdon, UK

[1]Institute for Energy Research - Plasma Physics,Forschungszentrum J¨ulich, Association EURATOM-FZJ, Trilateral Euregio Cluster, 52425 J¨ulich, Germany
[2]EURATOM-CCFE Fusion Association, Culham Science Centre, OX14 3DB, Abingdon, OXON, UK
[3]Laboratoire de Physique des Plasmas-Laboratorium voor Plasmafysica, Association EURATOM Belgian State, ERM/KMS, B-1000 Brussels, Belgium
[4]Instituto de Plasmas e Fusão Nuclear/IST, Associacao EURATOM-IST, Avenue Rovisco Pais, 1049-001 Lisbon, Portugal
[5]Ecole Polytechnique, LPP, CNRS UMR 7648, 91128 Palaiseau, France
[6]Max-Planck-Institut f¨ur Plasmaphysik, EURATOM-Assoziation, D-85748 Garching, Germany
[7]FOM institute DIFFER, Association EURATOM-FOM, P.O.Box, 1207, 3430BE, Netherlands
** See annex of F. Romanelli et al, "Overview of JET Results", (24th IAEA Fusion Energy Conference, San Diego, USA (2012)).*

Preprint of Paper to be submitted for publication in Proceedings of the 24th IAEA Fusion Energy Conference (FEC2012), San Diego, USA 8th October 2012 - 13th October 2012

ABSTRACT.
Disruptions are a critical issue for ITER because of the high thermal and magnetic energies that are released on short time scales, which results in extreme forces and heat loads. The choice of material of the plasma facing components (PFCs) can have significant impact on the loads that arise during a disruption. With the ITER-like wall (ILW) in JET made of beryllium in the main chamber and tungsten in the divertor, the main finding is a low fraction of radiation. This has dropped significantly with the ILW from 50-100% of the total energy being dissipated in the plasma with CFC to less than 50% on average and down to just 10% for VDEs. All other changes in disruption properties and loads are consequences of this low radiation: long current quenches, high vessel forces caused by halo currents and toroidal current asymmetries as well as severe heat loads. Temperatures close to the melting limit have been locally observed on upper first wall structures during deliberate VDE and even at plasma currents as low as 1.5MA and thermal energy of about 1.5MJ only. A high radiation fraction can be regained by massive injection of a mixture of 10%Ar with 90%D_2. This accelerates the current quench and by this reducing halo and sideways impact. The temperature of PFCs stays below 400^{o}C. MGI is now a mandatory tool to mitigate disruptions in closed-loop operation for currents at and above 2.5MA in JET.

1. INTRODUCTION

Disruptions are a critical issue for ITER because of the high thermal and magnetic energies that are released on short time scales, which results in extreme forces and heat loads being capable of damaging plasma facing components (PFCs) [1]. The new wall in JET with its main chamber material beryllium and the divertor made of tungsten [2] is a unique test bed to study disruptions under ITER-like conditions. Indeed, as it is shown in this paper, the material of the plasma-facing components has significant impact on the disruption properties and related loads. But the wall material does not only affect the disruption properties, it also changes plasma performance and requires therefore adjustment of plasma control in order to avoid disruptions. Enhanced core radiation by sputtered tungsten is one of the new issues to be addressed by proper control of divertor temperature to prevent from radiative collapse. Also density control has changed with the ITER-like wall (ILW), requiring more gas feeding to achieve sufficient density to avoid locked error field modes. The density limit itself has changed as well. Not only the H- to L-mode back transition occurs at higher densities, but also the dynamics of the density limit slowed down, giving more time to react and to prevent from disruptions. Most of these new control issues causing disruptions in the early phase of the ILW have been solved during the campaigns in 2011/2012. Disruptions also impact on machine conditioning by creating or mobilising dust and by loading PFCs with deuterium and impurities. This had significant impact on the breakdown and performance of subsequent pulses with carbon wall, but has become negligible with the ILW. These disruption related topics are discussed in more detail in [3, 4]. This paper will mainly focus on the disruption itself, namely its properties, resulting loads and their mitigation.

2. DISRUPTION PROPERTIES

The most important difference between the ILW and PFCs made of carbon is the absence of radiating impurities during the disruption process. This has significant implications: a) low radiation during the current quench phase, b) a hot current quench plasma, c) long current decay times, d) high heat loads caused by conduction of magnetic energy to PFCs, e) higher impact on the vacuum vessel by halo currents and current asymmetries. Figure 1 shows in a nutshell all of the above mentioned features for two representative disruptions, one with CFC wall and the other with the ILW.

2.1 RADIATION

The total stored energy in the plasma, consisting of magnetic energy W_{mag} and thermal energy W_{th}, is dissipated during a disruption through up to four loss channels. It can be radiated (W_{rad}), coupled into vessel and poloidal field coils ($W_{coupled}$), conducted to PFCs (W_{cond}) or partly converted to runaway electrons (W_{RE}):

$$W_{th} + W_{mag} = W_{rad} + W_{coupled} + W_{cond} + W_{RE} \quad (1)$$

The coupled energy is calculated from the current decay using a lumped parameter model for the mutual inductance, which includes energy flow to the vessel and the divertor coils [5, 6]. For fast current quenches (CQ), the coupled energy amounts to 50% and to 30% for very long current decays. In the following, we consider only disruptions without runaway generation. Figure 2 shows the total energy being radiated during the disruption as measured by bolometry as function of the total energy available in the plasma: $W_{th} + W_{mag} - W_{coupled}$. Most of the data points with CFC wall are above 50% radiation fraction, whereas with the ILW radiation is mainly below 50%. Lowest radiation fractions of about 10% are found during vertical displacement events (VDE).

The impurities that radiate during the current quench are mainly released during the thermal quench (TQ). It has been shown that especially the heat flux into the inner divertor plays a significant role on releasing carbon from deposited layers [7]. Strong layer formation is absent with the ILW. Dust being mobilised / created during the disruption has been measured by the high resolution Thomson scattering diagnostic (HRTS) in JET, which records the light emission from dust particles being hit by the intense laser beam [8]. With the ILW, the amount of dust is reduced by a factor 10 to 100 compared to CFC. This is in agreement with the strong reduction in radiation as the amount of released particles is very low, which adds to the effect of low radiation efficiency of Be.

2.2 TIMESCALES

Important for the mechanical but also thermal loads is the timescale of the current quench. The energy dissipation in the current quench is governed by the following power balance:

$$\frac{d}{dt}W_{mag} = -P_{coupled} - P_{ohmic}$$

$$\frac{d}{dt}W_{th} = P_{ohmic} - P_{rad} - P_{cond} \quad (2)$$

The magnetic energy is dissipated by inductive coupling and ohmic heating. The thermal energy is governed by the balance between ohmic heating and radiation. As long as the radiated power P_{rad} balances the ohmic heating P_{ohmic}, the current quench time is defined by the radiated power. When P_{rad} becomes comparable to the conductive loss P_{cond} , the characteristic time for thermal transport starts to play a role. Thus for low radiation fractions as seen with the ILW, long current decays are expected, whereas with CFC short current quenches should dominate. This is indeed the case as shown by the statistics in figure 3. The linear current decay times extrapolated from a 80% to 20% current decay and normalised to the area of the plasma cross section shows a distribution maximum for CFC wall at 3ms/m^2, whereas the distribution is much broader and clearly shifted to longer CQ times for the ILW. A substantial fraction of more than 30% of the disruption with ILW has decay times with more than 20ms/m^2.

2.3 ELECTRO-MAGNETIC LOADS

Vertical forces on the vacuum vessel can arise by induced eddy currents and poloidal halo currents. Additionally, m = n = 1 kink modes during the current quench give rise to sideways forces [9]. The halo current fraction I_H/I_P increases the larger the vertical displacement is at a certain plasma current during the CQ. This dependence is the same for both, ILW and CFC. As seen in figure 4, the maximum level of I_H/I_P is the same for both wall types. But the majority of disruptions with CFC has a fast current quench time compared to the vertical displacement time and has therefore a low halo current fraction. With the ILW, high halo current fractions are found at longer CQ times, whereas with the CFC high I_H/I_P is found for shorter τ_{CQ}. The reason for this is most likely a combination of faster vertical displacement and higher plasma resistivity with CFC. CQ times exceeding 100ms are recorded for the ILW mainly in cases, where the plasma column kept stable. Naturally, these mainly low triangularity pulses show a low I_H/I_P.

The impact on the vessel is not only defined by the maximum of I_H/I_P or the amplitude of the current asymmetries caused by the kink mode, but also by the length the force by these two is applied [3]. Figure 5 shows that the vessel displacement in vertical and radial direction increases with the halo current and sideways impulse. The longer current quenches with the ILW yield higher impulse and therefore larger vessel displacement. The vertical displacement is not only caused by halo currents, but also by eddy currents induced during the vertical movement. Therefore in addition to the total amplitude of the displacement the displacement in upward direction only is shown in figure 5. The latter is due to the halo current impact and can be well described by the motion of a mass-spring system. The high triangularity pulses shown have the highest vertical growth rates and are being vertically displaced after the TQ, resulting in ”cold” VDEs. In CFC the fast CQ time is limiting the halo current and sideways impact. For ILW, the impact of both can be significantly higher as the maximum amplitude is reached for longer CQ times.

2.4 THERMAL LOADS

Severe heat loads have been observed with the ILW during the current quench because of the lack of radiating impurities [7]. Looking again on equations 2, we find if P_{rad} is sufficiently low, the thermal energy during the CQ is not negligible and $P_{cond} = W_{th}/\tau_{th}$ becomes an important loss channel. The energy being conducted (or convected) to PFC, W_{cond}, is calculated from the energy balance (eq. 1). This energy is on average higher for ILW compared to CFC. However, the heat load impact, namely the temperature rise on PFCs, depends not only on the energy, but also on the deposition time scale and the wetted area. Figure 6 shows W_{cond} as function of the characteristic loss time of the magnetic energy, $\tau_{mag} = 0.5 \times \tau_{CQ}$, which gives an upper limit of the heat deposition time. Disruptions with CFC tend towards low W_{cond} and short τ_{mag}. With the ILW, W_{cond} can be very high. As long as τ_{mag} is sufficiently long, the temperature rise can be expected to be low. However, for those disruptions experiencing vertical displacement during the CQ, the deposition time can be short whilst W_{cond} is high. Beside cold VDEs, this is especially the case for hot VDEs as they show the lowest level of radiation. Such disruptions have the potential to cause localised melting of the Be PFCs at the upper wall protection of JET as it was observed by in-vessel video inspection. During the CQ of these disruptions, one or more temperature peaks are observed with the IR camera. Figure 6b shows the maximum temperature rise during these events, which is clearly correlated to $W_{cond} \times \tau_{mag}^{-1/2}$. But it has to kept in mind that this ΔT does not necessarily directly reflect the energy being deposited. The dashed red line indicates the average correlation, resulting in a wetted area of $3m^2$, the black dashed line is the most severe envelope of the data with $A_{wetted} = 1.75m^2$. Further analysis of IR data is necessary to directly estimate the wetted area. Clearly this can vary strongly depending on the movements of the plasma column. Additionally, as mention above, τ_{mag} is only an upper limit for the deposition time. It can be significantly shorter, when for example instabilities during the CQ cause a fast loss of thermal energy being stored in the current quench plasma.

2.5 RUNAWAYS

Runaway electron (RE) formation has not yet been seen so far in disruptions with the ILW [10]. This can be due to both, small toroidal electric fields because of slow current decay and/or strong MHD during these slow current quenches. Virtually all non-MGI disruptions have toroidal electric fields which are outside the domain of electric and magnetic fields for which runaway formation was observed with CFC wall (see figure 3 in [11]). A reliable recipe to generate runaways in a disruption with CFC wall was the injection of argon through a standard gas inlet into a limiter plasma at high magnetic field. An exact repeat of a reference pulse at 3T and 2.0MA has been tried with the ILWwall, showing no signs of runaway formation. The maximum current decay rate was 45MA/s only for 5.3×10^{20} injected Ar atoms, whereas with CFC the rate was three times higher, 145MA/s with 6.6×10^{20} Ar atoms. This can again be attributed to carbon release which adds to the radiation from the injected argon and accelerates the CQ further. The repeat with the ILW showed in addition strong magnetic fluctuation, which are known to cause prompt loss of high energy particles.

3. MITIGATION BY MASSIVE GAS INJECTION

Massive gas injection is studied in JET as a tool for mitigation since 2008 [6]. With CFC wall, various gases have been used: argon, neon, mixtures of those with 90% D_2 and helium. The injection of pure Ar and Ne let in many cases to the generation of runaway electrons. For the first campaigns with the new ILW, it was chosen to use only D2 mixtures to avoid RE formation. The severe loads observed with the ILW, especially the heat loads during the current quench phase, made the use of MGI mandatory in pulses with plasma current of $\geq$ 2.5MA. It is important to note that with the ILW no non-sustained breakdowns occurred after injection of D_2 mixtures in contrast to CFC wall. Severe impact of MGI on the performance of subsequent pulses has not been observed, however, a detailed analysis as has been done for CFC [12] is an open task.

3.1 MITIGATION EFFICIENCY

A high radiation fraction ranging between 70% and 100% of the plasma energy is being radiated with MGI in both, CFC and ILW (see figure 2). Scatter in the data arises from the injected species and the injection time during disruptions. A significant difference in radiation fraction between CFC and ILW is not observed, but it is seen that MGI with ILW tends towards slightly higher current decay times (cf. figure 3).

A detailed study of the impact of thermal energy on radiation efficiency has been done with the ILW by varying the fraction of thermal energy W_{th}/W_{tot} using different NBI input power up to 18MW but also different plasma current. Figure 7 shows the radiation fraction for high injection rate (valve pressure about p_{DMV} = 3.3MPa), low injection rate (p_{DMV} = 0.3 MPa) and for pure D_2 injection at high pressure. The radiation efficiency for pure D_2 is much lower compared to the Ar + D_2 mixture and also lower compared to D_2 with CFC wall, the latter showing that carbon contributed significantly to the total radiation. But also for the mixture, the radiation fraction drops from almost 100% for only ohmically heated pulses down to 70% at $W_{th}/W_{tot} \approx 0.5$. The drop is less severe for higher injection pressure. The decay in W_{rad}/W_{tot} with increasing fraction of thermal energy indicates that mitigation is less efficient during the TQ. A linear fit gives a radiation efficiency in the TQ of only 50% for maximum injection rate. It is important to note, that the radiation is measured 90° toroidally away from the injection point. This has to be taken into account, as toroidal asymmetries are likely during MGI, especially in the pre-TQ and TQ phase. The measurements only represent the average radiated energy if asymmetries are negligible or if the toroidal distribution is such that the measurement position is giving the average radiation. It is therefore difficult to distinguish a drop in radiation efficiency from a variation in the toroidal distribution. Therefore, a second bolometer has been used to estimate the radiation at 135° from the injection point. Because both bolometers differ in geometry (see [13]) only a simplified estimate for the total radiated power could be used. However, both bolometers give the same trend with W_{th}/W_{tot}, which leads us to the conclusion that indeed a degradation of the radiation efficiency is taking place.

MGI with D_2 mixtures reduces the generation or mobilisation of dust by roughly two orders

of magnitude for CFC and by about a factor of 2 on average with the ILW. It reduces halo current and sideways impact by decreasing the current quench time, resulting in smaller vessel displacement (cf. figure 5). With the ILW, MGI can lead to higher amplitudes of the vertical displacement compared to CFC with the same halo current impulse. This is because of higher eddy current forces due to the very fast current quenches with MGI. The upward displacement related to the halo currents is virtually zero with MGI. Heat loads during the CQ are suppressed sufficiently because of the high radiation efficiency during the CQ and therefore low W_{cond} (cf. figure 6). Temperature measurements with IR cameras during MGI are disturbed by IR emission from the plasma. However, extrapolating the temperature decay on PFCs after the disruption shows that temperatures stay below 400^{o}C.

A more detailed comparison of the current quench times is given in figure 8. The current quench time shows an increase with plasma current as the amount of injected gas is kept constant, pointing towards constant fuelling efficiency. The increase in τ_{CQ} is due to the increased ohmic heating during the CQ and can be reproduced by balancing ohmic power and radiated power using the simple current quench model introduced in [7] (dashed lines). Input to this model is the initial plasma current and the impurity density. The CQ times are found to be slightly longer with the ILW, which can be attributed to a finite contribution to the radiation by carbon with CFC wall and confirms the general trend seen in figure 3. The higher estimate of the argon density with CFC is therefore an artefact.

3.2 CLOSED LOOP OPERATION

The disruption mitigation valve (DMV) [14, 15] is presently triggered by basic but robust disruption detection signals. These are either the amplitude of a locked n = 1 mode or an excursion of the loop voltage, indicating the start of the CQ. The present system includes a longer delay caused by interlocks for the heating systems, which can be up to 50ms. Figure 9 shows an example of an actively mitigated disruption. The DMV was triggered by the modelock signal, which at the same time starts a soft stop sequence including reduction of plasma shaping and current. Injection takes place during the CQ as indicated by the drop in voltage in the DMV power supply ($U_{PS,DMV}$), leading to a clear acceleration of the current decay, a stop of the upward displacement and consequently a low halo current fraction.

During the ILW campaigns 2011-2012 67 unintentional disruptions were mitigated by MGI. During the commissioning phase of the closed-loop operation, 5 disruptions were missed due to inhibits in the real-time protection system. Incorrect setting of the timing caused 4 missed disruptions. Taking human error and commissioning phase into account, the success rate is about 88%. Due to the type of trigger and due to the long interlock delay, all MGIs in closed-loop injected the gas after the first thermal quench. Mitigation was still successful with respect to CQ loads, because of the slow current decay. However, the TQ has not been mitigated, which is only acceptable because the thermal energy dropped by that time to values typical for ohmic heating only. For the coming campaigns in 2013, the interlock delay will be shortened and new schemes for triggering have to be established to ensure also TQ mitigation.

4. SUMMARY, CONCLUSIONS & OUTLOOK

The use of beryllium for the first wall and tungsten in the divertor has shown a strong reduction of the radiation during disruptions compared to the previously installed CFC wall. This results in slower current quench rates and consequently in higher halo current and sideways impact as well as in extreme heat loads at still moderate stored energies. For ITER this means that the heat loads occurring during the thermal quench will be enhanced by conductive losses during the current quench. High radiation fractions can be regained by MGI, which is essential to protect the ILW from melting. However, although the mitigation efficiency with respect to heat loads is by far sufficient for JET, the low radiation efficiency during the TQ is worrying and far from the ITER requirements of 90% radiation fraction. A second DMV is planned to be installed in JET in 2013 at the outer midplane. This will give the opportunity to study the impact of multiple injection and injection location on mitigation efficiency.

ACKNOWLEDGEMENTS

This work was supported by EURATOM and carried out within the framework of the European Fusion Development Agreement. The views and opinions expressed herein do not necessarily reflect those of the European Commission.

REFERENCES

[1]. Sugihara M et al., 24th IAEA Fusion Energy Conference, San Diego, USA (2012) ITR/P1-14.
[2]. Matthews G F et al., ”Plasma operation with metallic walls”, 20th International Conference on Plasma Surface Interactions, Aachen, 2012, submitted to Journal Nuclear Materials.
[3]. de Vries P C et al., ”The impact of the ITER-like wall at JET on disruptions”, 39th European Physical Society Conference on Plasma Physics (EPS2012), Stockholm, Sweden.
[4]. Huber A et al., ”Impact of the ITER-like Wall on Divertor Detachment and on the Density Limit in the JET Tokamak”, 20th International Conference on Plasma Surface Interactions, Aachen, 2012, submitted to Journal Nuclear Materials.
[5]. Riccardo V et al., Plasma Physics and Controlled Fusion **44** (2002) 905.
[6]. Lehnen M et al., Nuclear Fusion **51** (2011) 123010.
[7]. Lehnen M et al., ”Disruption heat loads and their mitigation in JET with the ITERlike wall”, 20th International Conference on Plasma Surface Interactions, Aachen, 2012, submitted to Journal Nuclear Materials.
[8]. Giovannozzi E et al., Review of Scientific Instruments **81** (2010) 10E131.
[9]. Gerasimov S N et al., 39th EPS Conference on Plasma Physics Stockholm, July 2 - 6, ECA 36F, P-5.074 (2012)
[10]. Plyusnin V V et al., 24th IAEA Fusion Energy Conference, San Diego, USA (2012)
[11]. Lehnen M et al., Journal Nuclear Materials **390-391** (2009) 740.
[12]. Kruezi U et al., Journal Nuclear Materials **415** (2011) S828.

[13]. Huber A et al., Fusion Engineering and Design **82** (2007) 13271334.
[14]. Kruezi U et al., 36th EPS Conference on Plasma Physics Sofia, June 29 - July 3, ECA 33E, P-2.153 (2009).
[15]. Reux C et al., 27th Symposium on Fusion Technology (SOFT) , Liege, Belgium 2012.

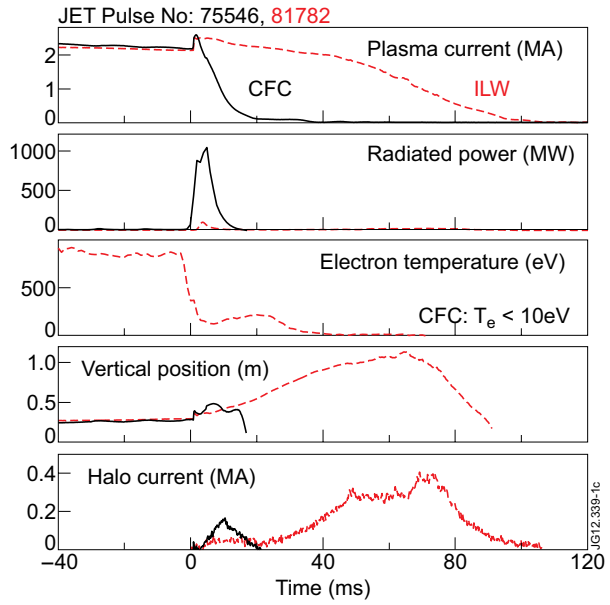

Figure 1: Comparison of two disruptions with CFC and ILW, which reflect the typical changes with introduction of a metallic wall.

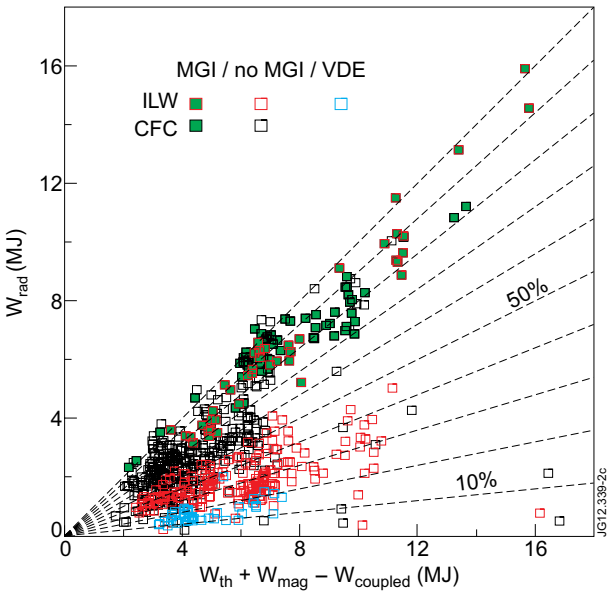

Figure 2: Radiated energy as function of the energy available in the plasma.

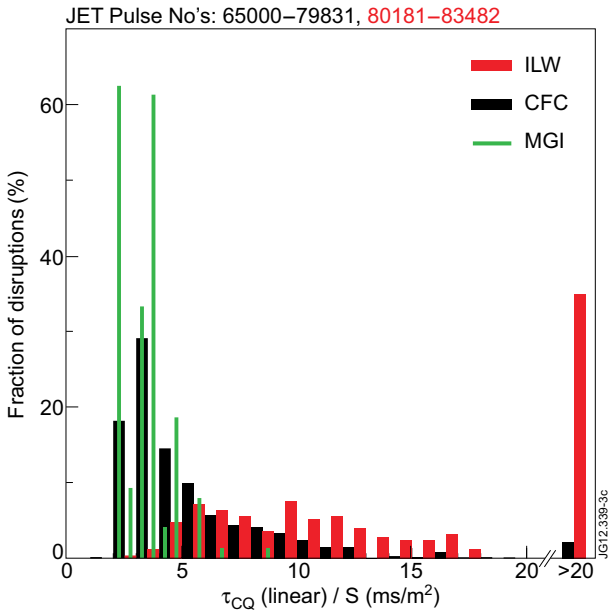

Figure 3: Current quench times excluding disruptions with runaways.

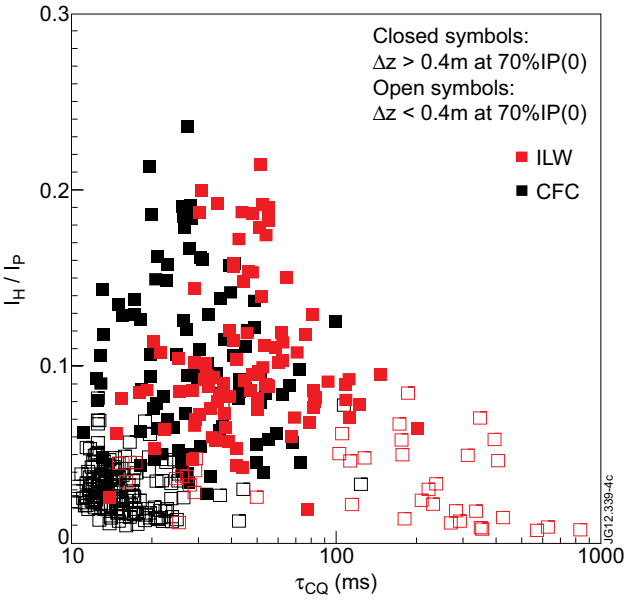

Figure 4: Halo current fraction as function of the linear current quench time excluding hot VDEs.

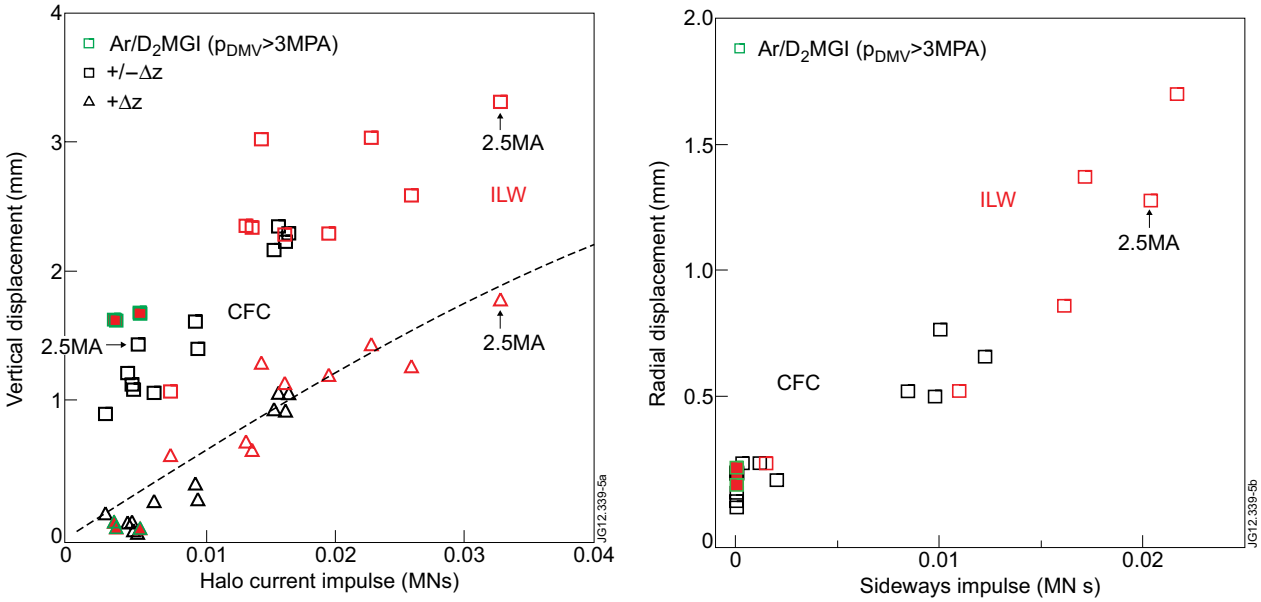

Figure 5: Vertical and radial vacuum vessel displacement as function of halo current and sideways impact. All data for 1.8MA < I_p< 2.2MA except stated otherwise. The dashed line is the vertical displacement calculated for a mass spring system with f = 14Hz and m = 180t.

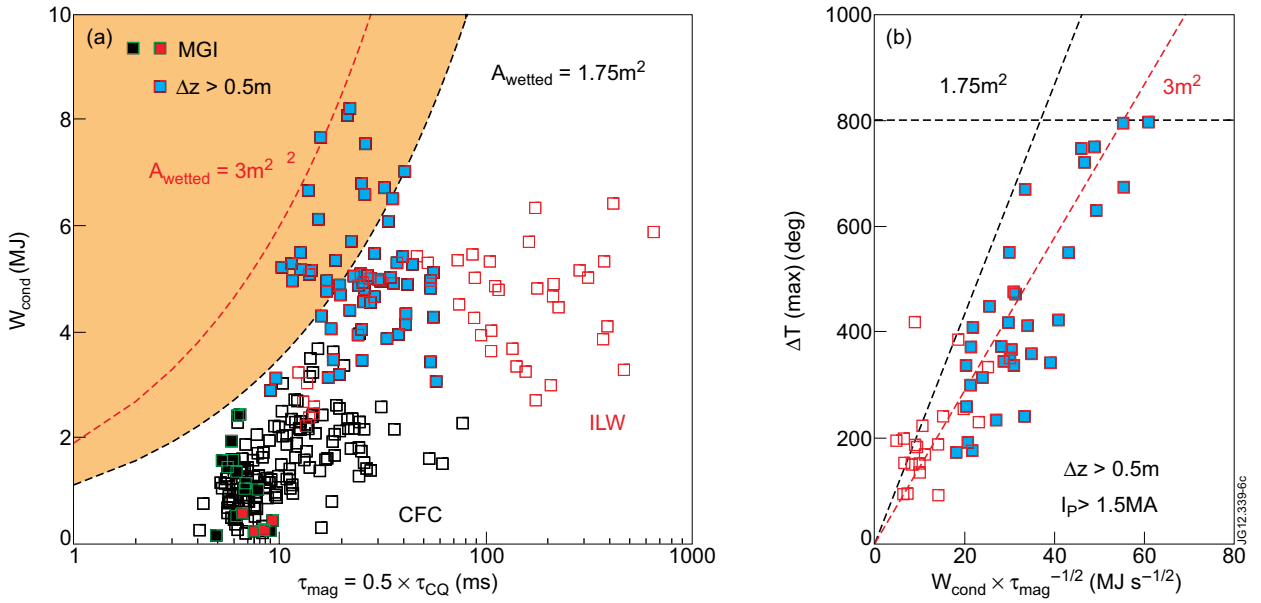

Figure 6: Heat load for disruptions with W_{th}/W_{mag}< 0.1. a) Energy that is conducted/convected during the disruption as function of the loss time of the magnetic energy ($\tau_{mag} = \tau_{CQ}/2$). Dashed lines indicate the melting limit for Be of 25MJm^{-2}s$^{-1/2}$. b) Maximum temperature rise on upper inner wall protection limiter and dump plate during the disruption.

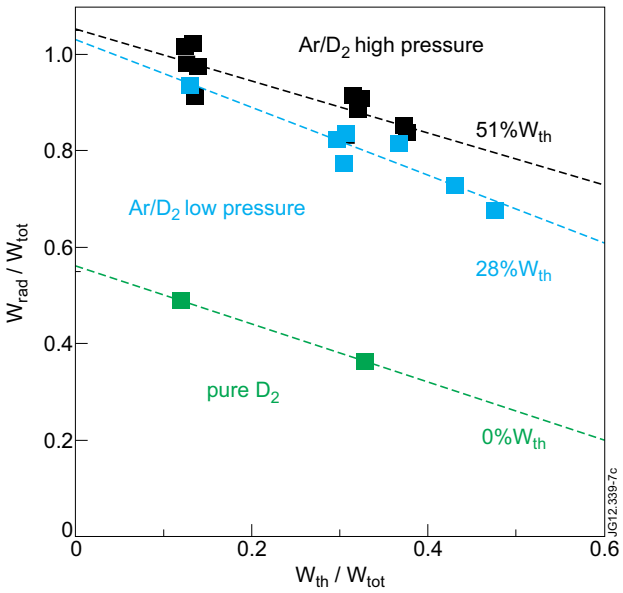

Figure 7: Radiated energy during MGI as function of the fraction of thermal energy stored in the plasma before injection.

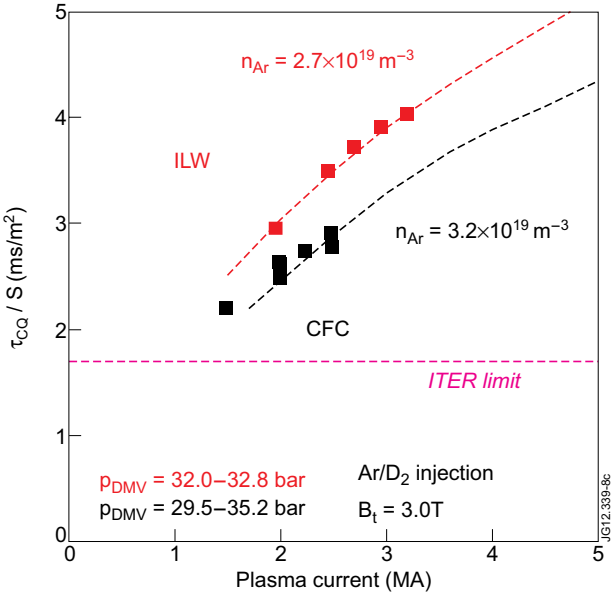

Figure 8: Linear current quench time extrapolated from 80% to 20% current decay as function of plasma current. Dashed lines are from current quench model.

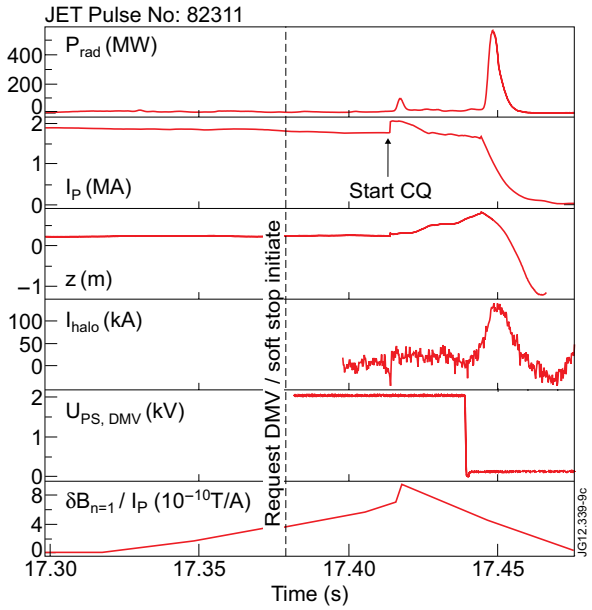

Figure 9: Example of closed loop operation of the DMV with p_{DMV} = 3.2MPa and Ar + D_2 injection.